Proceedings of OMAE 2006
25th International Conference on
Offshore Mechanics and Arctic Engineering
June 04-09, 2006, Hamburg, Germany



OMAE2006-92323

# THE ROBUSTNESS OF THE ADDED MASS IN VIV MODELS

**Leandro D. Cunha**
Departamento de Engenharia Mecânica
Escola Politécnica da USP
Brasil
leandro.cunha@poli.usp.br

**Celso P. Pesce***
Departamento de Engenharia Mecânica
Escola Politécnica da USP
Brasil
ceppesce@usp.br

**Juan Wanderley**
Departamento de Engenharia Naval e Oceânica
Universidade Federal do Rio de Janeiro
Brasil
juanw@peno.coppe.ufrj.br

**André L.C. Fujarra**
Departamento de Engenharia Naval e Oceânica
Escola Politécnica da USP
Brasil
afujarra@usp.br

## ABSTRACT

*In this paper we show that added mass coefficient, $C_a$, is robust, i.e., is a first measure of model consistency. Regardless of the model type, phenomenological as well as CFD models, the general trend of the added mass coefficient plot is always the same.*

## NOMENCLATURE

$\alpha, b, \gamma$ calibration parameters of model I
$\alpha_0, \alpha_1, \alpha_2, \alpha_3, \alpha_4$ calibration parameters of model II
$A, \varepsilon, \gamma, C_{L0}$ calibration parameters of model III
$b$ viscous damping
$\delta_v$ the ratio $\omega_v/\omega_s$
$\delta_w$ the ratio $\omega_w/\omega_s$
$C_a$ added mass coefficient
$k$ elastic spring stiffness
$m_a$ effective added mass
$m_a^p$ potential added mass
$m_s$ structural mass
$m^*$ mass ratio
$\omega_{ob}$ observed vibration frequency
$\omega_s$ vortex shedding frequency
$\omega_v$ natural frequency in vacuum
$\omega_w$ natural frequency in still water
$St$ strouhal number
$U_r = V_r = U^*$ reduced velocity
$\zeta_w$ nondimensional damping in still water

## INTRODUCTION

In the present paper we use the results of added mass coefficient obtained from a linear oscillator model as a basis of comparison to analyse results from several phenomenological VIV models (all of them based in van der Pol type nonlinear equations) and from a numerical CFD VIV model. The linear oscillator is monochromatically forced by an ideal source. An expression for the resulting added mass coefficient is taylored from the well known results available in the linear systems theory. The resulting expression perfectly recovers the Added Mass general trend which is composed of: a) Large values of $C_a$ at the beginning of lock-in; b) the zero in the curve at resonance frequency; c) the trailing asymptote derivative approaching 0; d) the asymptotic tendency to $C_a = -1$ for large values of reduced velocity.

*Address all correspondence to this author.

The experimental results of Vikestad et al. and of Fujarra as well as the numerical results of Wilden and Graham are used to show the general trend thus cited.

In the sequence, the phenomenological models of VIV developed by Hartlen and Currie, 1970, Iwan and Blevins, 1974, and Facchineti *et al.*, 2004, are presented and the results of their direct numerical simulation are shown. Some key plots of the models simulations help to understand the behavior of the added mass coefficient in each model studied. Also, the results of a particular CFD model is shown. All the results show a common pattern regardless of experimental apparatus, numerical method or even the exact form of a phenomenological model.

The comparison of the added mass coefficient plots thus obtained uncovers the main conclusion of this work which is the robustness of the added mass coefficient among all analysed models. The work proceeds to the mathematical analysis of the phenomenological models equations. The lack of a closed form solution of the equations does not enable one to present an expression analogous to the case of the forced linear oscillator. Nevertheless, at least in first order, the coupled (van der Pol)-(linear elastic) oscillators behave like a forced linear elastic oscillator. This fact is used to partialy explain the robustness pointed out.

This study is restricted to 1-dof cross-flow VIV phenomena.

## ADDED MASS IN VIV

The linear ordinary differential equation describing the transversal oscillations, in the $Y$ direction, of a rigid cylinder is given by:

$$m_s\ddot{Y} + b\dot{Y} + kY = F_{tot}(t) \tag{1}$$

The oscillations are forced by the term $F_{tot}(t)$ which is the transversal component of the force due to the effects of fluid flow. This force is the integral of the pressure and friction over the cylinder surface. $F_{tot}(t)$ could be decomposed in two components: $F_a(t)$, in phase with the cylinder acceleration, $\ddot{Y}$; and $F_v(t)$, in phase with the cylinder velocity, $\dot{Y}$:

$$F_{tot}(t) = F_a(t) + F_v(t) \tag{2}$$

The inertial component of $F_{tot}(t)$ can be rearranged in equation Eqn. (1) which is then modified to:

$$(m_s + m_a)\ddot{Y} + b\dot{Y} + kY = F_v(t) \tag{3}$$

$$m_a\ddot{Y} = -F_a(t) \tag{4}$$

The quantity, $m_a$, defined by equation Eqn. (4) is the added mass. The time series for $F_{tot}$ and $\ddot{Y}$ can be obtained by physical experiments, numerical simulation of CFD models and numerical simulation of phenomenological models. The resulting added mass from these three sources will be shown and compared in the following sections.

## ADDED MASS CALCULATED FROM EXPERIMENTAL SIGNALS

Experimental data compiled in added mass coefficient plots suggest evidences of considerable robustness as could be seen in Figs. 1 and 3.

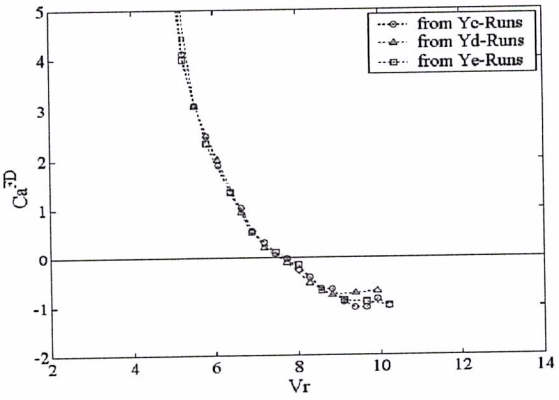


Figure 1: ADDED MASS COEFFICIENT CALCULATED FROM EXPERIMENTAL RESULTS USING FREQUENCY DOMAIN METHODS. EXTRACTED FROM FUJARRA [1]. $Vr$ VALUES ARE BASED on $\omega_w$

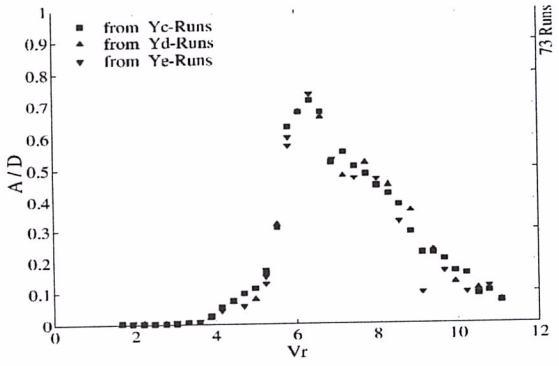


Figure 2: TRANSVERSE AMPLITUDE RESPONSE CORRESPONDING TO FIG. 1. EXTRACTED FROM FUJARRA [1]. $Vr$ VALUES ARE BASED on $\omega_w$.

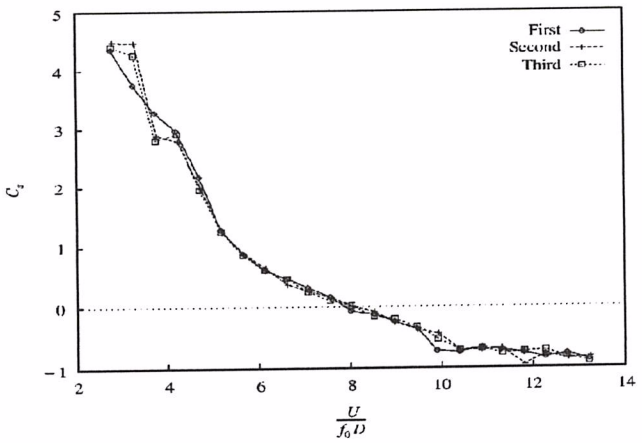


Figure 3: ADDED MASS COEFFICIENT CALCULATED FROM EXPERIMENTAL RESULTS USING TIME DOMAIN METHODS. EXTRACTED FROM VIKESTD *et al.* [2]. $Vr$ VALUES ARE BASED on $\omega_v$.

From the above added mass plots the following noticeable characteristics could be enumerated:

1. The added mass coefficient, $C_a$, takes large values as the reduced velocity, $U_r$, approaches low values;
2. $C_a$ approaches zero as $U_r \approx 8$;
3. as $U_r$ grows, $C_a$ approaches the value $-1$ asymptotically.

They also illustrate different methods to obtain the added mass coefficient from time series data. While Vikestad *et al.* relies on some assumed mathematical properties of the signals in time domain, Fujarra uses a general technique based on Fourier transforms of the signals [3]. This explains the superscript $FD$, in Fig 1, which stands for *frequency domain*. Also, as can be drawn from these two graphics, $C_a$ values show considerable scattering at both lower and higuer $U_r$ values, where diplacements take small values.

## ADDED MASS FROM IDEAL SOURCE FORCING

Equation (1) can be simulated using ficticious time functions playing the role of $F_{tot}(t)$. The linear system is then said to be forced by an ideal source since its response does not interfere in the dynamics of the forcing. A particularly interesting case is that of pure sinusoidal functions. In this section, all $U_r$ values are based on $\omega_v$.

The value of $m^*$ is used to normalize the amplitude of $F_{tot}(t)$ since $F_{tot}(t)$ amplitude is made to be inversely proportional to $m^*$. The value of $\zeta$ is used directly in Eqn. (1). Table 1 shows the values of the parameters that are used in the simulations.

As well known, Fig. 4 shows that the value of $\zeta$ interferes only with the peak amplitude reached during resonance while the value of $m^*$ affects mostly the residual vibration amplitude

Table 1: PLOTS KEY

| Symbol | $m^*\zeta$ | $m^*$ | $\zeta$ |
|---|---|---|---|
| $\star$ | 0.33 | 10 | 0.033 |
| $\circ$ | 0.033 | 10 | 0.0033 |
| $\bullet$ | 0.0033 | 3.3 | 0.001 |

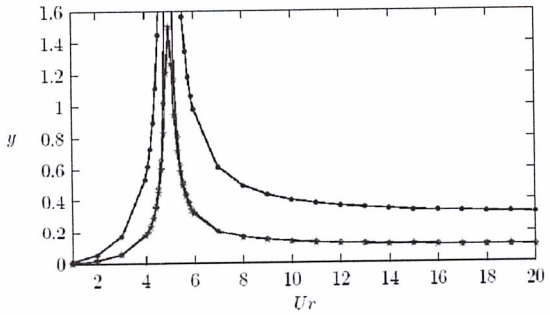


Figure 4: AMPLITUDE RESPONSE OF A LINEAR SYSTEM FORCED BY AN IDEAL SOURCE.

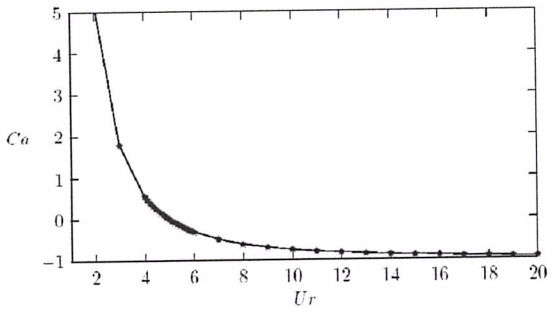


Figure 5: ADDED MASS COEFFICIENT OF A LINEAR SYSTEM FORCED BY AN IDEAL SOURCE.

at high $U_r$ values. From Fig. 5, it is seen that the added mass coefficient is an invariant of the forced system. Figures 4 and 5 were extracted from [4].

## ADDED MASS FROM PHENOMENOLOGICAL MODELS

The equations defining the phenomenological models presented by Hartlen and Currie [5], Iwan and Blevins [6] and

Facchineti *et al.* [7] are shown below in normalized form, Eqns. (5)-(10). The model presented by Iwan and Blevins was revisited by Parra and Aranha [8] and the equations used in this work are the same presented there. Those are, respectively, refered to as model I, model II and model III. One could observe that the nonlinear equations representing the fluid dynamics, Eqns. (6), (8) and (10), are in van der Pol form. Also, of importance, the equations are dimensionless and length and time were brought to nondimensional form through the cylinder diameter and the shedding frequency, $\omega_s$, respectively. In this section, all $U_r$ values are based in $\omega_v$, the natural frequency in vacuum.

**Model I: Hartlen and Currie [5]**

$$\ddot{y} + 2\zeta_w \delta_w \dot{y} + \delta_w^2 y = \frac{1}{2\pi^3 St^2 (m^* + 1)} \int_{t_0}^{t} v dt + \frac{1}{m^* + 1} \ddot{y} \quad (5)$$

$$\ddot{v} + \alpha(3\frac{\gamma}{\alpha} v^2 - 1)\dot{v} + v = b\delta_v \ddot{y} \quad (6)$$

**Model II: Iwan and Blevins [6]**

$$\ddot{y} + 2\zeta_w \delta_w \dot{y} + \delta_w^2 y = \quad (7)$$

$$\frac{1}{2\pi^3 St^2 (m^* + 1)} \frac{\alpha_4}{\sqrt{\alpha_2}} (v - 2\pi St \sqrt{\alpha_2}\, \dot{y}) + \frac{1}{m^* + 1} \ddot{y}$$

$$\ddot{v} + 2\alpha_1 (4v^2 - 1)\dot{v} + v = \frac{2}{\pi} \frac{\alpha_4 \sqrt{\alpha_2}}{\alpha_0} \ddot{y} \quad (8)$$

**Model III: Facchineti *et al.* [7]**

$$\ddot{y} + 2\zeta_w \delta_w + \delta_w^2 y = \frac{C_{L0}}{2\pi^3 St^2 (m^* + 1)} v - \frac{\gamma}{\mu} \dot{y} \quad (9)$$

$$\ddot{v} + \varepsilon(v^2 - 1)\dot{v} + v = A\ddot{y} \quad (10)$$

Figures 6 to 11 were extracted from [4] and show the results of the numerical simulation corresponding to each phenomenological model. The simulation was directly implemented using standard programming techniques [9–11]. The equations were solved, the resulting time series were interpolated, a FFT was applied and finally important information was extrated.

Models I and II were originally presented using the Rayleigh form for the wake oscillators. The Rayleigh to van der Pol transformation is classic and, in VIV context, may be found in [12]. The tranformation of model I to van der Pol form introduces an integral term as can be seen in Eqn. (5). This integral term introduces an offset in the resulting time series causing difficulties in the subsequent signal processing. The Rayleigh form for the wake oscillator was used in the numerical solver. Despite the form used to simulate the model, the van der Pol form was used to present the models equations in order to allow for direct comparation of the models. Additional details can be found in [4].

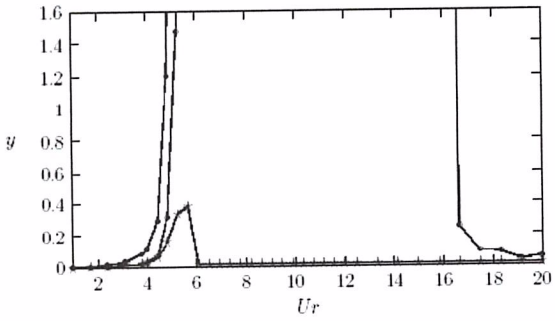


Figure 6: AMPLITUDE RESPONSE OF MODEL I.

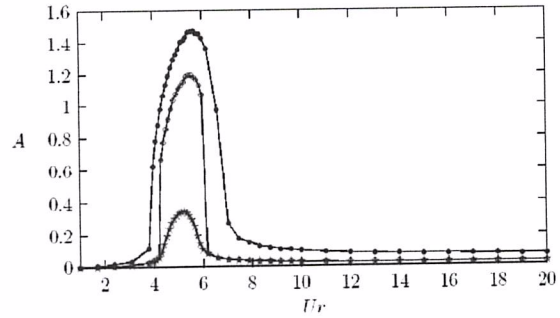


Figure 7: AMPLITUDE RESPONSE OF MODEL II.

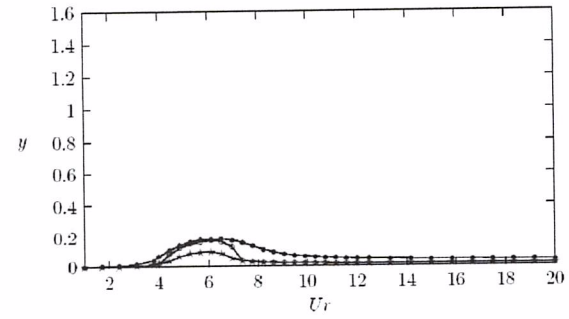


Figure 8: AMPLITUDE RESPONSE OF MODEL III.

The same set of values for $m^*$ and $\zeta$ are used in the simulation of all three models. The particular parameter values are shown in Tab. 1, presented above.

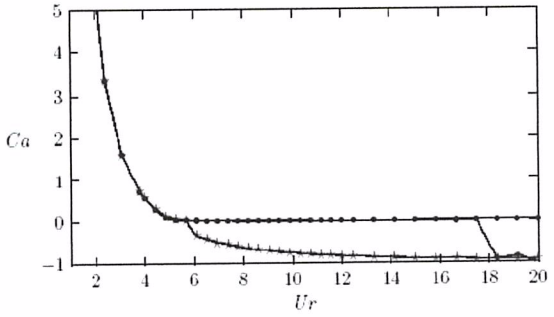


Figure 9: ADDED MASS COEFFICIENT OF MODEL I.

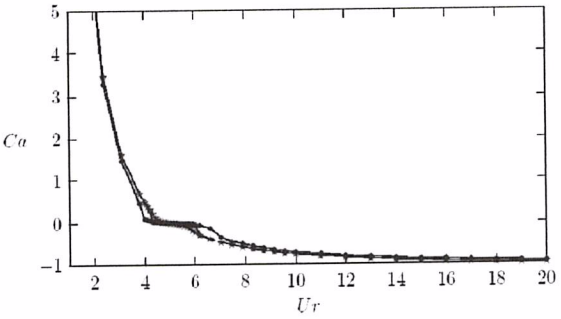


Figure 10: ADDED MASS COEFFICIENT OF MODEL II.

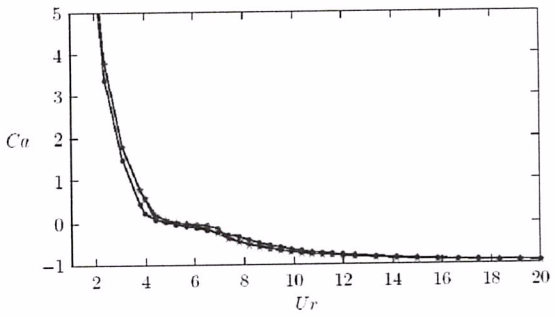


Figure 11: ADDED MASS COEFFICIENT OF MODEL III.

The simulation shows that all three phenomenological models are able to represent the VIV lock-in. Model I which was calibrated from Feng's data [13], according to [5], appears not to have universality as it predicts very large amplitude responses for low values of the parameters $m^*$ and $\zeta$. Possible explanations for this behavior of model I are the lack of a stall term, see [7, 14], and the restricted set of calibration parameters. Model II shows an amplitude response curve with peak values close to those observed in experiments. Model III shows peak amplitude response values far lower than those observed in experiments.

The experimental data show null added mass at reduced velocity $\approx 8$. Whereas, all three phenomenological models studied herein show the added mass coefficient taking values close to zero as the amplitude response shows lock-in. Reasons for such a discrepancy will be addressed in the sequel.

## ADDED MASS FROM CFD MODELS

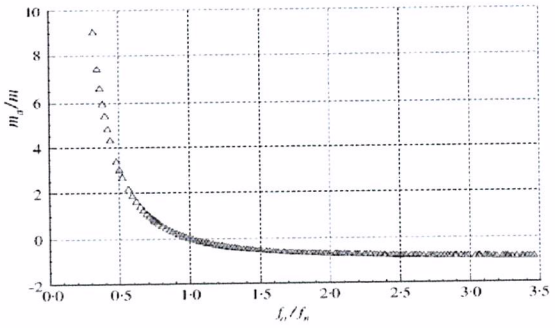


Figure 12: ADDED MASS COEFFICIENT OF THE WILLDEN AND GRAHAM CFD NUMERICAL MODEL. EXTRACTED FROM WILLDEN AND GRAHAM [15].

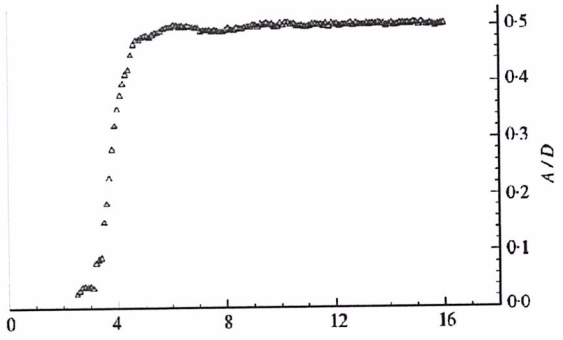


Figure 13: AMPLITUDE RESPONSE VERSUS REDUCED VELOCITY OF THE WILLDEN AND GRAHAM CFD NUMERICAL MODEL. ADAPTED FROM WILLDEN AND GRAHAM [15]. $U_r$ VALUES ARE BASED $\omega_v$.

As can be seen in Fig. 12, the added mass calculated by Willden and Graham from a numerical CFD model is remarkably close to the added mass coefficient obtained from a linear system forced by an ideal source. The quantity $f_0/f_n$, expressed

in the figure, corresponds to $U_r/5$ (as Strouhal number, $St$, was taken to be 0.2). Figure 13 shows the amplitude response. Interestingly, the plot presents a persistent vibration amplitude even when the reduced velocity is raised to values as high as 16.

## DISCUSSION

The discussion below has no intention to be comprehensive, neither conclusive, but just to highlight some interesting aspects regarding the $C_a$ curve. The closeness of the Willden and Grahan added mass numerical data to that of the forced linear model is remarkable, since the CFD simulation solves strongly nonlinear equations. Data from Fig. 12 were reploted into Fig. 5, yielding Fig. 14, to emphasize their proximity. Reasons for this behavior could only be guessed in this work since we compare only one CFD result. Nevertheless, this discussion raises questions about how a highly nonlinear model responds almost like a linear one.

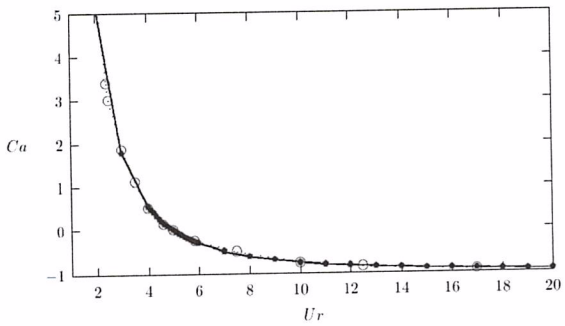


Figure 14: ADDED MASS COMPARATION OF CFD AND LINEAR MODELS. SYMBOL ○ SHOWS DATA ADAPTED FROM WILLDEN AND GRAHAM [15]. $U_r$ VALUES ARE BASED $\omega_w$.

The $C_a$ plots of the phenomenological models are close enough to its linear (first order) part, that was presented in Fig. 5, except for the results near resonance frequency , *i.e.*, in the flat regions around $U_r = 5$ in Figs. 10 and 11, and for $U_r > 5$ in Fig. 9.

A forced van der Pol oscillator exhibits a locking between the response frequency and the resonance frequency when the forcing frequency is near that of resonance, as could be seen in [16]. Let β represent the detuning parameter in a forced van der Pol oscillator, *i.e.*, the ratio between the forcing frequency and the oscillator's natural frequency. The study of forced van der Pol oscillators show that when the detuning parameter is close to one the oscillator resonates, pulsating with its own natural frequency, a phenomena known as locking. This locking is here pointed out as the source of the near zero behavior of $C_a$ given by those models when $U_r \approx 5$, *i.e.*, near resonance.

### The Zero Value of the $C_a$ Curve

Also, from experimental results, the $C_a$ zero value is seen to occur near the transition from the upper to the lower branch. This transition happens when the system oscillation frequency is passing through $\omega_v = 2\pi f_{vacuum}$, the resonance frequency in vacuum, see Fig. 15. Figure 15 gives the outline of the amplitude response given by 1-dof VIV. On the other hand, 2-dof VIV gives rise to more complex phenomena that cannot be summarized in a 2D figure see [17–19]. The added mass calculated from the forced linear oscillator shows a zero value exactly when the forcing is passing through resonance, *i.e.*, when $U_r = 5$. At this point, one must stress that $C_a = 0$ is related to $U_r$ values at which the VIV system vibrates near its resonance frequency in vacuum. Nonetheless there is a discrepancy between the values observed experimentally, $U_r \approx 7.5$, and the value predicted by the linear model, $U_r = 5$. The reason for such a discrepancy is not yet clear.

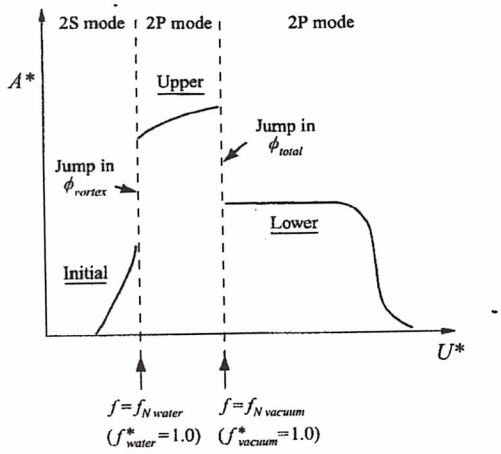


Figure 15: TYPICAL LOW $m^*\zeta$ AMPLITUDE RESPONSE SHOWING THE RELATION OF JUMP PHENOMENA TO DIFFERENT RESONANCE FREQUENCIES. EXTRACTED FROM [20].

### Behavior within the Lower-Branch

Another point that should be observed is the absence of a clear flat region in the experimental $C_a$ plots within the lower-branch. In fact, as there is a clear relationship between the observed oscillation frequency, $\omega_{ob}$, and the calculated added mass as could be seen in Eqn. (11); refer to [2,4]. It could be deduced that, when the $C_a$ is constant, $\omega_{ob}$ should also be constant.

$$\omega_{ob} = \omega_{vacuum}\sqrt{\frac{m^*}{m^* + C_a}} \tag{11}$$

It is shown in [20] that the observed vibration frequency is constant along the lower-branch. As a consequence, one should observe a flat, constant region, in $C_a$ curves calculated from experimental results. However, this behavior is not observed in Figs. 1 and 3.

### Behavior at Low Reduced Velocities

Clearly, from all experimental and theoretical $C_a$ plots presented, there is no finite asymptotic value as $Ur \rightarrow 0$. This raises the following question: shouldn't the well-known $C_a = 1.0$ value, experimentally observed in still fluid, be recovered from those plots? A plausible answer is: not necessarily, as all the data over which the $C_a$ was calculated, being them numerical (CFD) or analytical (phenomenological models), refer to a Karman street flow regime, which is structurally distinct from the very low-velocity flows, i.e., at very-low Reynolds number, where separation does not exist.

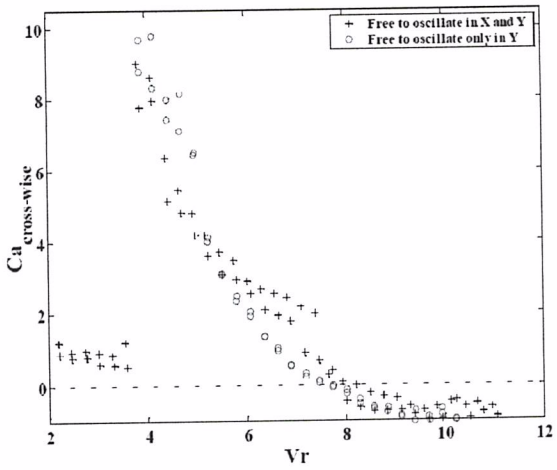


Figure 16: $C_a$ PLOT CALCULATED FROM EXPERIMENTAL DATA SHOWING A DISCONTINUITY AT LOW REDUCED VELOCITIES. EXTRACTED FROM [21].

However, the experimental results in Fig. 16 shows a region, at reduced velocities below the lock-in, with a different behavior. The tendency to $C_a = 1$ is noticeable. This plot combines the results from two experiments: in one of them, the streamwise vibration is restrained, and in the other, the body is free to oscillate in 2-dof. Note that, at low reduced velocities, the data plotted is related to a 2-dof experiment.

## CONCLUSION

The most significant result of this analysis on added mass is the observation of the similar response achieved from all experiments, linear models, phenomenological models and CFD models. The added mass general trend is recovered from all models and experiments, *i.e.*, a) Large values of $C_a$ at the beginning of lock-in; b) the zero in the curve at resonance frequency; c) the trailing asymptote derivative approaching 0; d) the asymptotic tendency to $C_a = -1$ for large values of reduced velocity).

Despite the diferences amongst the various models amplitude responses, the added mass plots show little deviation from the general trend thus identified. For the experimental results, there are minor differences among the experiments but this could be caused by variations in the experimental setups and facilities. The added mass coefficient plot is an invariant for the ideally forced linear model. Most notable, is the similarity between the presently addressed CFD $C_a$ plot and the ideally forced linear model results. For the phenomenological models, there is a range near $U_r = 5$, where the added mass coefficient is near zero, clearly related to the predicted lock-in range.

Finally, the authors argue that any lack in recovering the general trend in the added mass coefficient should be interpreted as a strong sign of inconsistency of a given model, an expected result.

## ACKNOWLEDGMENT

The authors acknowledge the USP (Universidade de São Paulo), FAPESP (Fundação de Amparo à Pesquisa do Estado de São Paulo) and FINEP (Financiadora de Estudos e Projetos) for their support in this research.

## REFERENCES

[1] Fujarra, A., 2002. "Analytical and experimental studies of vortex induced vibrations in rigid and flexible cylinders". PhD Thesis - in Portuguese, Universidade de São Paulo.

[2] Vikestd, K., Vandiver, J., and Larsen, C., 2000. "Added mass and oscillation frequency for a circular cylinder subjeted to vortex induced vibrations and external disturbance". *Journal of Fluids and Structures,* **14**.

[3] Pesce, C., and Fujarra, A., 2002. "Added mass of an elastically mounted rigid cylinder in water subjected to vortex-induced vibrations". In Proceedings of OMAE.

[4] Cunha, L., 2005. "Vortex induced vibration: Critical analysis of phenomenological models". MS Thesis - in Portuguese, Universidade de São Paulo, December.

[5] Hartlen, R., and Currie, I., 1970. "Lift oscillator model of vortex induced vibration". *Proceedings of the ASCE.*

[6] Iwan, W., and Blevins, R., 1974. "A model for vortex-induced oscillation of structures". *Journal of Applied Mechanics,* **41**.

[7] Facchineti, M., Biolley, F., and de Langre, E., 2004. "Coupling of sructure and wake oscillators in vortex induced vibrations". *Journal of Fluids and Structures,* **19**.

[8] Parra, P., and Aranha, J., 1996. Vortex induced vibrations: Phenomenological models and experiments. Technical report written in portuguese, Escola Politécnica da USP.

[9] Stallman, R., and Developers, 2005. *Using GNU Compiler Collection*. Free Software Foundation. See also URL `http://www.gnupress.org`.

[10] Stallman, R., and McGrath, R., 2005. *The GNU make Manual.* Free Software Foundation. See also URL `http://www.gnu.org/software/make/`.

[11] Galassi, M., 2005. *GNU Scientific Library Reference Manual*, 2nd ed. Free Software Foundation. See also URL `http://www.gnu.org/software/gsl/`.

[12] Sarpkaya, 1979. "Vortex induced vibrations". *Journal of Fluids and Structures,* **9**.

[13] Feng, C., 1968. "The measurement of vortex-induced effects in flow past stationary and oscillating circular and d-section cylinders". MS Thesis, University Of British Columbia.

[14] Skop, R., and Balasubramanian, S., 1997. "A new twist on an old model for vortex-induced vibrations". *Journal of Fluids and Structures,* **11**.

[15] Willden, R., and Graham, J., 2001. "Numerical prediction of viv on long flexible circular cylinders". *Journal of Fluids and Structures,* **41**.

[16] Stoker, J., 1950. *Nonlinear vibrations in mechanical and electrical systems.* Interscince.

[17] Williamson, C., and Jauvtis, N., 2004. "A high amplitude 2T mode of vortex-induced vibration for a light body in xy motion". *European Journal Mechanics B/Fluids,* **23**.

[18] Williamson, C., and Govardhan, R., 2004. "Vortex-induced vibrations". *Annual Reviews in Fluid Mechanics,* **36**.

[19] Pesce, C., and Fujarra, A., 2005. "The 'super upper branch' VIV response of flexible cylinders". In Proceedings of the 3$^{rd}$ BBVIV.

[20] Govardhan, R., and Williamson, C., 2000. "Modes of vortex formation and frequency response of a freely vibrating cylinder". *Journal of Fluids Mechanics,* **420**.

[21] Fujarra, A., and Pesce, C., 2004. "Vortex-induced vibration with a 2-dof elastically mounted cantilevered cylinder in water: Some results on cross and stream-wise added mass". In Proceedings of the FIV.